Biomedical Physics & Engineering Express

ENDORSED BY IPEM Institute of Physics and Engineering in Medicine

PAPER • OPEN ACCESS

LIPUS far-field exposimetry system for uniform stimulation of tissues *in-vitro*: development and validation with bovine intervertebral disc cells

To cite this article: Devante A Horne *et al* 2020 *Biomed. Phys. Eng. Express* **6** 035033

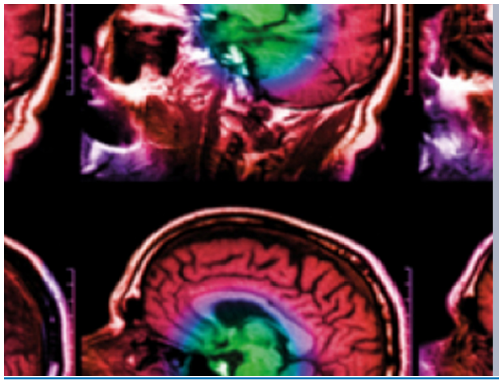

Biomedical Physics & Engineering Express

PAPER

LIPUS far-field exposimetry system for uniform stimulation of tissues *in-vitro*: development and validation with bovine intervertebral disc cells

Devante A Horne[1,2,3], **Peter D Jones**[3], **Matthew S Adams**[3], **Jeffrey C Lotz**[1,2] and **Chris J Diederich**[2,3]

[1] Department of Orthopaedic Surgery, University of California, San Francisco, United States of America
[2] The UC Berkeley—UCSF Graduate Program in Bioengineering, University of California, Berkeley, and University of California, San Francisco, United States of America
[3] Thermal Therapy Research Group, Radiation Oncology Department, University of California, San Francisco, United States of America

E-mail: chris.diederich@ucsf.edu

Keywords: low-intensity pulsed ultrasound, LIPUS, ultrasound exposimetry, intervertebral disc, annulus fibrosus, nucleus pulposus, *in-vitro*

OPEN ACCESS

RECEIVED
2 January 2020

REVISED
8 April 2020

ACCEPTED FOR PUBLICATION
20 April 2020

PUBLISHED
30 April 2020

Abstract

Therapeutic Low-intensity Pulsed Ultrasound (LIPUS) has been applied clinically for bone fracture healing and has been shown to stimulate extracellular matrix (ECM) metabolism in numerous soft tissues including intervertebral disc (IVD). In-vitro LIPUS testing systems have been developed and typically include polystyrene cell culture plates (CCP) placed directly on top of the ultrasound transducer in the acoustic near-field (NF). This configuration introduces several undesirable acoustic artifacts, making the establishment of dose-response relationships difficult, and is not relevant for targeting deep tissues such as the IVD, which may require far-field (FF) exposure from low frequency sources. The objective of this study was to design and validate an in-vitro LIPUS system for stimulating ECM synthesis in IVD-cells while mimicking attributes of a deep delivery system by delivering uniform, FF acoustic energy while minimizing reflections and standing waves within target wells, and unwanted temperature elevation within target samples. Acoustic field simulations and hydrophone measurements demonstrated that by directing LIPUS energy at 0.5, 1.0, or 1.5 MHz operating frequency, with an acoustic standoff in the FF (125–350 mm), at 6-well CCP targets including an alginate ring spacer, uniform intensity distributions can be delivered. A custom FF LIPUS system was fabricated and demonstrated reduced acoustic intensity field heterogeneity within CCP-wells by up to 93% compared to common NF configurations. When bovine IVD cells were exposed to LIPUS (1.5 MHz, 200 μs pulse, 1 kHz pulse frequency, and $I_{SPTA} = 120$ mW cm^{-2}) using the FF system, sample heating was minimal (+0.81 °C) and collagen content was increased by 2.6-fold compared to the control and was equivalent to BMP-7 growth factor treatment. The results of this study demonstrate that FF LIPUS exposure increases collagen content in IVD cells and suggest that LIPUS is a potential noninvasive therapeutic for stimulating repair of tissues deep within the body such as the IVD.

Introduction

Ultrasound (US) can deliver mechanical or thermal energy to induce therapeutic effects including hyperthermia, ablation, regeneration or remodeling, enhanced local drug delivery, and immunotherapy [1–5]. Devices for these purposes can be distinguished by their dimensions and position relative to the body, driving frequency and acoustic waveforms, as well as spatial-temporal intensity and pressure profiles, all of which largely dictate the distribution of the acoustic energy delivered and the effects on tissue. Low-intensity pulsed ultrasound (LIPUS) is one therapeutic US approach that is applied in pulsed wave modes with relatively low average intensities, thereby generating little to negligible heating and primarily delivering mechanical energy [3]. Therapeutic LIPUS has been shown to have significant regenerative capabilities in

numerous tissue types through stimulation of cellular proliferation and matrix metabolism [6–16]. Recently, with U.S. Food and Drug Administration approval for bone fracture healing, LIPUS has advanced into the clinic as a noninvasive and regenerative therapy.

Interest in therapeutic LIPUS has expanded in recent years with evidence that LIPUS may also stimulate repair of injuries in soft tissues including cartilage, ligament, tendon, and intervertebral disc (IVD). Several *in-vivo* studies have demonstrated LIPUS-induced enhancement of wound healing by stimulating increased collagen synthesis and alignment, tissue integration, and improved biomechanical function including enhanced stiffness and failure strength [17–21]. Additionally, LIPUS has been shown to promote matrix anabolism in IVD cells by increasing collagen and glycosaminoglycan synthesis while simultaneously decreasing matrix metalloproteinase expression [22]. Yet, there is little known about the mechanism of its effects at the cellular level, nor which other cell or tissue types may respond to LIPUS exposure. The Exogen® clinical system, and other experimental devices, have been used to evaluate LIPUS bioeffects [23–29], with the majority of published work focused on the established exposure settings for bone healing (1.5 MHz; 200μs pulse; delivered at 20% duty cycle (1 kHz); I_{SATA} 30 mW cm^{-2} ; 20 min daily). Investigations of LIPUS bioeffects at other exposure settings, such as at frequencies below 1.0 MHz and acoustic intensity profiles representative of far-field (FF) delivery, are limited and may be required for acoustic energy to penetrate to deep tissues such as the human IVD.

In-vitro testing systems have been developed for preclinical assessment of therapeutic US under controlled experimental conditions. In the most common LIPUS configuration, cells are exposed by placing a commercial polystyrene cell culture plate (CCP) containing cellular material in the acoustic near-field (NF), directly on top of the US transducer with acoustic coupling gel. While a simple and straightforward approach, this configuration is vulnerable to several undesirable acoustic artifacts including NF interference, standing wave formation, and uncontrolled temperature elevation [30]. These phenomena represent significant confounding factors when attempting to establish dose-response relationships [31]. Many groups have studied US fields in CCPs [30–35]. Hensel *et al* (2011) investigated the wave propagation characteristics of several typical *in-vitro* configurations. They reported that reproducibility was negatively affected by reflecting surfaces (i.e. allowing standing wave formation), and that small differences in system configuration, such as well size, media volume, and alignment with beam axis can significantly affect the acoustic field distribution and ultimately the biological response. Further, the effect of uncontrolled temperature fluctuations due to direct heating from contact with the US transducer as well as absorption of US-energy and heating within the plastic well-bottom and sidewalls can be particularly problematic. LIPUS systems have previously been developed to address these confounding factors. Fung *et al* (2014) varied the acoustic standoff distance of their *in-vitro* LIPUS system and found that osteocytes were sensitive to the axial distance of LIPUS, suggesting that FF US exposure could enhance osteogenic activities. In the system developed by Marvel *et al* (2010), BioFlex CCPs with flexible well-bottoms were used and found to be more acoustically transparent than typical polystyrene CCPs. In the 2014 study by Leskinen *et al*, the authors found that there was substantial temperature variation among different wells within a CCP, and that this variation correlated with variations in cell behavior. They found that temperature elevations were minimal when using a CCP well area larger than the width of the US beam [36]. Additionally, several LIPUS studies have implemented the use of an acoustic absorber placed above the CCP well to attenuate standing wave formation [30, 33, 35, 37]. These results highlight the importance of characterizing parameter- and configuration-specific acoustic field distributions and temperature fluctuations during *in-vitro* LIPUS exposure.

In consideration of investigating extracorporeal delivery of LIPUS to deep tissue targets such as IVDs, lower than typical transducer operating frequencies and focused or uniform FF exposure are assumed technical requirements. The objective of this study was to design and characterize an *in-vitro* LIPUS system that mimics attributes of a deep delivery system, and as such delivers uniform, FF acoustic energy profiles while minimizing reflections and standing waves within target wells and unwanted temperature elevation within target samples. Further, the system was validated by exposing IVD cells and assessing LIPUS-induced biological effects.

Methods

System design and characterization

To meet the primary objective of maximizing FF acoustic dose uniformity at the location of the target sample in the *in-vitro* setup, CCP dimensions, transducer dimensions, and offset distance between the transducer surface and the CCP-well were determined. Two CCP setups were evaluated, each with an effective cell culture area of 1.91 cm^2. One setup included a narrow 24-well plate (15.6 mm diameter), and the other a wider 6-well plate (34.8 mm diameter) with a custom toroidal spacer (15.6 mm inner diameter). This spacer serves to constrain the cells within the CCP-well center while limiting exposure to sidewall acoustic reflections and maintaining a small volume similar to the 24-well plate. To identify the ideal separation distance from the transducer to the CCP-well (acoustic standoff) for specific CCP well coverage, several constraints were imposed: (i) the acoustic standoff must place the target sample beyond the heterogeneous NF; (ii) the full width at half

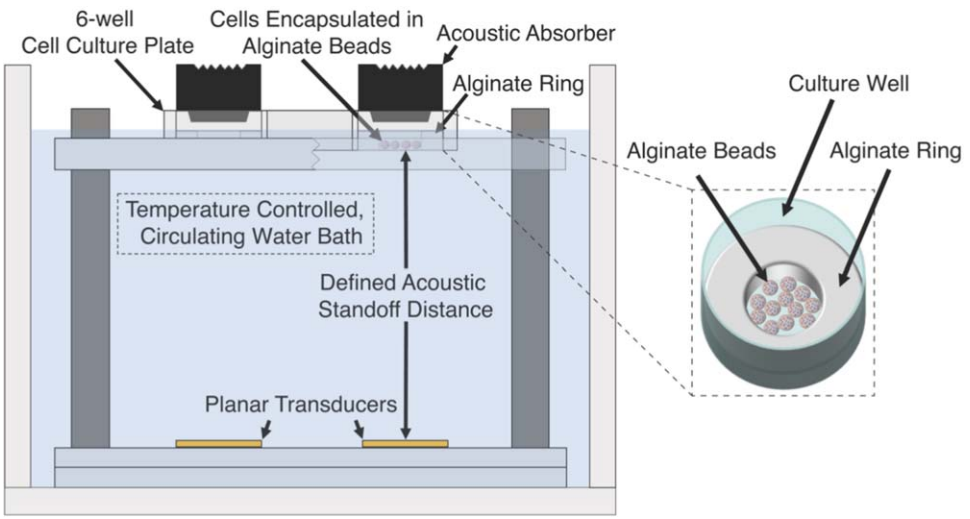

Figure 1. Generalized schematic representing the *in-vitro* LIPUS system designed to deliver uniform acoustic energy to cells cultured in monolayer or 3D scaffolds and to adapt to a frequency range from 0.5 to 1.5 MHz. Two planar, PZT transducers were directed toward the center of two opposing corner wells of a standard cell culture plate. Cell culture targets were placed at a defined acoustic standoff distance and within an acoustically transparent alginate ring spacer to center the cells and reduce exposure to sidewall acoustic reflections. Wells were sealed distally with an acoustic absorber coupled to the media. The system was placed in a degassed, temperature-controlled water bath during exposures.

maximum (FWHM), or 50% contour of beam maximum, must cover at least 80% of the effective cell culture area (1.91 cm^2); and (iii) the acoustic standoff distance and minimum transducer size must be constrained to avoid an excessively divergent field and potential well-wall absorption and reflections.

Specification and characterization of transducers

Transducer specifications were identified by investigating a range of transducer diameter (20–35 mm), frequency (0.5, 1.0, and 1.5 MHz), and acoustic standoff distance within the FF (120–400 mm) on corresponding US intensity distributions, uniformity, and coverage area based upon acoustic field simulations. Full-field acoustic intensity distributions were calculated using the rectangular radiator method [38] for numerical approximation to the Raleigh-Sommerfield diffraction integral, applying methods previously described by our group [39], and assuming uniform velocity across the transducer surface.

Planar disc PZT US transducers of 25 mm diameter (EBL #1, EBL Products, Inc., East Hartford, CT, USA), with a resonant frequency of approximately 0.5, 1.0, or 1.5 MHz, were selected. Transducer assemblies were fabricated separately with water-tight air-backing on custom 3D-printed housing fixtures, as designed in Solidworks (Dassault Systemes, Waltham, Massachusetts, USA) and printed using the Clear resin material with a Form 2 3D-printer (Formlabs Inc., Somerville, MA, USA). Black silicone adhesive sealant (Permatex 81158, Solon, OH, USA) was applied along the edge of the transducer to secure it to the fixture and ensure air-backing. Peak electrical impedance, zero phase cross-over, and resonance frequency for each transducer were measured using a Network Analyzer (E5070B ENA RF, Agilent). Acoustic beam plots of the intensity patterns for each transducer were acquired in the transverse plane using a custom 3D computer-controlled scanning system (Velmex, Bloomfield, NY, USA) with a calibrated hydrophone (HNP-0400, Onda Corp, Sunnyvale, CA, USA). Transducers were placed in a tank lined with an acoustic absorber to reduce reflections and filled with deionized, degassed water. A function generator (HP 33120A, Agilent, Santa Clara, CA, USA) and RF amplifier (ENI 240L) were used to drive transducers with a power meter (N1914A EPM, Keysight Technologies, Inc., Santa Rosa, CA, USA) and power sensor modules (N8482A, Keysight Technologies, Inc., Santa Rosa, CA, USA) in-line for monitoring forward and reflected power. For hydrophone measurements, a standard burst mode signal at the primary resonant frequency was used (1 kHz pulse repetition, 100–200 cycle burst). Hydrophone scanning step sizes were 0.2 mm $\times$0.5 mm across transverse and axial axes, respectively. The peak-to-peak voltage (Vpp) signal from the hydrophone was measured using a digital oscilloscope (DSOX2024A 200 MHz, Keysight Technologies, Santa Rosa, CA, USA) and converted to absolute intensity maps. Beam intensity distributions were calculated, normalizing the maximum intensity value to one in each case to provide a simplified comparison of distributions.

Assembly of LIPUS in-vitro system

Informed by the simulations and measurements described above, exposimetry systems were devised and fabricated in-house following the schema (figure 1). The LIPUS system consists of two independently driven, planar transducers mounted separately

Table 1. Candidate absorber materials and associated acoustical properties.

Product name	Density (g/cm^3)	Speed of sound (m/s)	Attenuation coefficient (dB/cm)	Reflection amplitude (mVpp)
Smooth-On Mold Star^{TM} 15 SLOW	12.36	1425.30	7.50	789.05
Smooth-On Mold Star^{TM} 30	13.00	1428.60	6.70	859.40
Smooth-On Dragon Skin^{TM}	6.71	1436.55	7.50	892.60
Smooth-On Ecoflex^{TM}	10.78	1444.38	1.77	1038.95
Dow Sylgard$^{®}$ 170	8.27	1433.70	18.44	253.90
Momentive^{TM} RTV60	8.47	1439.94	16.39	324.23

and affixed to an acrylic base. In order to operate with a single amplifier and function generator, paired transducers for each test system were individually impedance matched to a 100 Ω load using an LC matching network and connected in parallel to achieve 50 Ω resultant impedance. The matching network capacitance was adjusted slightly for final matching to equalize peak output intensities as measured by needle hydrophone. The CCP-platform was fixed at the identified acoustic standoff for each frequency, as described above, and the transducer position was adjusted to direct acoustic energy towards the center of two opposing corner wells of the CCP. In order to further reduce well-wall reflections and US beam refocusing as observed when using narrow-diameter 24-well plates, a wide-diameter 6-well CCP (Costar 3471, Corning Incorporated, NY, USA) was used. An alginate disk (34.8 mm diameter; 10 mm height) was formed by mixing equal volumes of 1.2 wt% sodium alginate (FMC BioPolymer, San Jose, CA, USA) and 102 mM $CaCl_2$ crosslinking solution inside each test well. Following 10 min incubation and removal of the crosslinking solution, a 3D-printed boring tool (15.6 mm outer diameter) was used to remove the center portion of the disk, creating an alginate ring. The acoustically transparent alginate rings (measured attenuation coefficient = 0 dB cm^{-1}) were used to constrain target samples within the FWHM of the diverging US beam and maintain a sample volume comparable to the 24-well plates without introducing reflective surfaces. Two custom silicone absorbers (described in detail below) were positioned apically and coupled on the distal surface of the media-filled target wells. During exposures, the entire setup was placed in a deionized, degassed, and temperature-controlled water bath, with the water level reaching one-half the height of the CCP.

Design of acoustic absorber

Acoustic absorbers were designed to be in direct contact with the top surface of the media as a means to absorb acoustic energy transmitted through the target and eliminate reflections and standing wave formation within the well. Six biocompatible silicone materials were evaluated based on measurements of acoustic attenuation and reflection due to acoustic impedance mismatch from water (table 1). Each material was prepared according to manufacturer's instructions, degassed, poured into cylindrical molds (4.2 cm diameter) to create two samples of different thicknesses (1.32 ± 0.10 cm and 2.55 ± 0.07 cm), and allowed to cure at room temperature overnight. Density was determined by using mass measurements and volume calculations. A pulse-echo transmit and receive US transmission system was used to determine the attenuation coefficient, reflection amplitude, and speed of sound through each material [40]. The test system consisted of an ultrasonic pulser-receiver (500PR, Panametrics, Inc., Waltham, MA, USA), two opposed 5 MHz immersion transducers (U8517054, Olympus NDT Instruments, Milwaukie, OR, USA) for transmit and receive, respectively, separated by 10 cm. The received amplitude waveform was measured using an oscilloscope (AFG3022C, Tektronix, Inc., Beaverton, OR, USA). Samples of various thickness were placed on a thin mylar stage between the two transducers and positioned perpendicularly to the US beam. The speed of sound through each sample C_s [m/s] was calculated as:

$$C_S = \frac{Z_1 - Z_2}{\left(t_{s,1} - t_{s,2} - \frac{Z_2 - Z_1}{Cw}\right)}$$

where Z_1 and Z_2 are the respective sample thicknesses [m] of sample 1 and sample 2, $t_{s,1}$and $t_{s,2}$ are the respective times [s] for the US signal to travel from the emitting transducer to receiving transducer, and C_w is the speed of sound [m/s] through water (1484 m s^{-1} at 22 °C). The attenuation coefficient of each sample μ [dB/m] was calculated as:

$$\mu = \frac{\ln\left(\frac{Ao,\,1}{Ao,\,2}\right)}{Z_2 - Z_1}$$

where $A_{o,1}$ and $A_{o,2,}$ are the respective peak-to-peak voltage amplitudes [V] measured from the pulse waveform, and Z_1 and Z_2 are the respective sample thicknesses [m]. Reflection amplitude was assessed by measuring the amplitude of the signal reflected back toward the emitting transducer. For each parameter assessed, measurements were taken four times in various positions throughout the sample and are reported as average values (table 2).

Table 2. Summary of acoustic field metrics from simulations of 0.5, 1.0, and 1.5 MHz transducers of various diameters. FWHM and % Area Covered was calculated for each offset distance. Only configurations that covered greater than 80% of a 24-well plate well bottom were considered to meet the design criteria; therefore, 25 mm diameter transducers and offset distances of 350, 250, and 125 mm were chosen for 1.5, 1.0, and 0.5 MHz frequency configurations, respectively.

Operating frequency (MHz)	Transducer diameter[a] (mm)	Offset distance (mm)	FWHM at offset (mm)	% Area covered[b]
	20	225	14.0	80.5
	25	300	12.2	61.2
1.5	25	350	14.2	82.9
	30	300	10.3	43.6
	35	300	9.3	35.5
	20	175	14.0	80.5
	20	200	16.0	105.2
1.0	25	225	14.0	80.5
	25	250	15.4	97.5
	20	300	19.2	75.5
	30	275	15.0	92.5
	30	400	20.0	81.9
	35	375	16.0	105.2
0.5	25	120	14.6	87.8
	25	125	16.2	107.3

[a] Distance from the center of the transducer face to the center of the measurement plane.

[b] Percentage of the surface area of a 24-well cell culture plate well bottom covered by the FWHM ultrasound beam (surface area of 24-well plate well bottom = 1.91 cm^2).

A custom mold was designed to create an absorber with the following characteristics: (i) a truncated-cone geometry (35.5 mm diameter x 8 mm depth; 25.4 mm total thickness) to allow direct coupling with media as well as air flow and media escape when placed in a media-filled well; and (ii) a ridged distal surface to baffle reflected waves, further increase absorption, and reduce re-transmission into the media. Mixed and degassed Sylgard 170 silicone (1696157, Dow Corning, Midland, MI, USA) was poured into a 3D-printed mold and cured by manufacturer's instruction. Pulse-echo measurements, similar to above, were performed to characterize the reflection amplitude of the final absorber design.

Characterization of US beam uniformity at cell culture position

US intensity distributions directly inside CCP-wells was characterized for various configurations. The full LIPUS assembly was placed in a scan tank and hydrophone measurements were performed inside the well at 2 mm above the bottom of the CCP, representing the location of the center of a 3D cell culture material. Six configurations were assessed, representing those commonly used for *in-vitro* LIPUS exposures [28, 30, 32, 34, 35, 41–43]: in the NF (no plate, 24-well CCP, and 6-well CCP) and in the FF (no plate, 24-well CCP, and 6-well CCP + alginate ring insert). Scan dimensions in the x-y plane were limited for some configurations due to narrow well diameter. As a quantitative measure of acoustic uniformity across the well area, the mean gradient magnitude was calculated using the numerical gradient function in the MATLAB Image Processing Toolbox (MATLAB Release 2016b, The MathWorks, Inc., Natick, MA, USA). The gradient vector magnitude was computed by the summation of the absolute value of the gradient vectors in the x and y dimensions.

Measurement of temperature elevation

Temperature elevation within the well and absorber was evaluated during LIPUS exposure. Copper-constantan thermocouples (Size 0.002in, California Fine Wire Company, Grover Beach, CA, USA) were fabricated and calibrated in-house and connected to a Data Acquisition/Switch Unit and Thermometry Modules (Model HP34970A, Keysight Technologies, Santa Rosa, CA, USA) set to one reading per second. Target wells contained a custom alginate ring and 10 alginate beads (3D cell culture scaffold material), all submerged in cell culture media (Dulbecco's modified Eagle's medium, Gibco; Invitrogen Inc., Carlsbad, CA, USA) which formed a liquid column inside the well. The acoustic absorber was partially submerged in the well as designed, coupling directly with the media while avoiding bubble formation. Multiple thermocouple probes were passed through the absorber and positioned parallel to the direction of US propagation in three different locations: centered and in contact with the well bottom, inside an alginate bead, and inside (2 mm from the bottom surface) the acoustic absorber. The full LIPUS assembly was submerged in a tank with water conditioned as described above and maintained at 37 °C. The top of the exposure system was covered with plastic sheeting to minimize heat and water vapor escape and to maintain temperature uniformity throughout the apparatus. LIPUS sonication was performed using the following parameters: 1.5 MHz operating frequency, 200 μs pulse, 1 kHz pulse repetition frequency, and $I_{SPTA} = 120\ mW\ cm^{-2}$. After a short baseline measurement, the LIPUS was switched on for 20-minute sonication followed by a cooldown back to steady-state. Measurements of temperature rise were repeated three times for each setup.

Biological validation of LIPUS system

The FF LIPUS system described above, operating at 1.5 MHz, was used to apply pulsed US *in-vitro* to IVD cells which were then assessed for induced biological response. Bovine IVD cells were encapsulated in 3D alginate scaffolds and cultured in 6-well CCPs. Samples were randomly assigned to the nontreated control, growth factor treatment (BMP-7) as a positive control, or LIPUS treatment group. After 14 days in culture, extracellular matrix accumulation within the alginate scaffold was evaluated by hydroxyproline assay for total

collagen content and dimethylmethylene blue assay for sulfated glycosaminoglycan content.

Cell culture

IVDs were harvested from 18 to 24-month old bovine tails (Marin Sun Farms Inc., Petaluma, CA, USA) and annulus fibrosus (AF) cells were extracted and expanded as previously described [44], then encapsulated in alginate beads. Alginate hydrogels are widely used as an encapsulation method in a variety of *in-vitro* applications, including chondrocyte [45, 46], fibroblast [47], and IVD [42, 48–51] cell culture, and have been used in several LIPUS studies involving IVD cells [28, 42, 52, 53]. The alginate bead culture system has many advantages over other hydrogel systems for IVD cell culture. AF cells cultured in alginate have been shown to maintain phenotypic stability [54, 55]. An additional advantage is that unlike many other hydrogels, alginate can be rapidly solubilized by calcium-chelating agents, allowing retrieval of viable cells while removing trace elements of the hydrogel material [54, 56]. Further, culturing samples in several beads rather than a single disc is advantageous as it facilitates the randomization of samples for various outcome assays following treatment. Extracted AF cells were suspended in 1.2 wt% sodium alginate (FMC BioPolymer) in D-PBS at a density of 4×10^6 cells/ml. Beads of approximately 25 μl in volume were formed by dispensing the solution dropwise through a 22-gauge needle into a reservoir of 102 mM $CaCl_2$ crosslinking solution. The beads were allowed to crosslink at room temperature for 10 min before washing with PBS and cell culture media. Twelve alginate beads (one sample) were cultured in two opposing corner wells of a CCP with 3 ml of Standard Disc Media (low-glucose DMEM with 5% FBS, 1% antibiotic/antimycotic, 1% nonessential amino acids, and 1.5% osmolarity salt solution containing 5 M NaCl and 0.4 M KCl). To avoid US exposure in neighboring, non-sonicated wells [30], each sample was cultured in opposing corner-wells, and control samples were not cultured in the same plate. Cells were kept in a 37 °C, 5% CO_2 incubator and allowed to acclimate for 24-hours before initial treatment.

Evaluation of LIPUS exposure

Twelve samples were divided among three groups: (1) nontreated control, (2) BMP-7 treatment, and (3) LIPUS treatment. The BMP-7 treatment group received Standard Disc Media supplemented with 200 ng ml^{-1} of Human Bone Morphogenetic Protein-7 (BMP-7) (Z02751, GenScript, Piscataway, NJ, USA). BMP-7 solution was exchanged on each treatment day. The LIPUS group was exposed to an US waveform (1.5 MHz operating frequency, 200 μs pulse, 1 kHz pulse repetition frequency, $I_{SPTA} = 120$ mW cm^{-2}) for 20 min each treatment day. When the CCP was placed on its platform, care was taken to remove air bubbles from and allow water to fill the crevices in the corners of the plate to allow proper coupling. To simulate environmental conditions without LIPUS, control and BMP-7-treated samples were placed in the LIPUS exposimetry system for 20 min with the US turned off. All samples were cultured for 14 total days, with LIPUS exposure taking place on 8 of the 14 days. Media was changed on each day of treatment or every other day.

Quantification of collagen concentration

After 14 days of culture, the alginate beads were dissolved in 55 mM sodium citrate. Samples were concentrated by lyophilization for 2 total hours at a minimum of 75 °C. Concentrated pellets were then dissolved in 40 μl of 6 N HCl for 16 h at 110 °C. The solution was centrifuged, and the supernatant was collected and neutralized. Total collagen content was quantified using acid hydrolysis followed by addition of p-dimethylaminobenzaldehyde and chloramine T (Sigma). DNA content was assayed with the Quant-iT PicoGreen dsDNA Assay Kit (P11496, Thermo Fisher, Waltham, MA, USA) and measured on a microplate reader (Spectramax M5, Molecular Devices, Sunnyvale, CA, USA) with 488 nm excitation and 525 nm absorption. Total collagen levels were normalized by the amount of total DNA to accommodate for differences in proliferation among treated and control samples.

Quantification of glycosaminoglycan concentration

After alginate beads were dissolved in 55 mM sodium citrate, the supernatant was digested in papain (P3125, Sigma-Aldrich, St. Louis, MO, USA) at 60 °C overnight. Sulfated glycosaminoglycan (sGAG) content was quantified using the dimethylmethylene blue (DMMB) assay, with modifications for measuring alginate encapsulated samples [57], and normalized by DNA content as measured by PicoGreen assay.

Statistical analysis

Statistical significance of differences in intensity gradient was evaluated using a one-way analysis of variance (ANOVA) test, followed by multiple *t*-tests with a Tukey HSD correction. Statistical significance of differences in collagen concentration was evaluated using the Kruskal-Wallis ANOVA test, followed by nonparametric comparisons for each pair using the Wilcoxon method. *P*-values < 0.05 were considered significant.

Results

Transducer and acoustic field characterization

Analysis of acoustic field simulations suggested that 25mm-diameter transducers would provide a practical selection for 0.5, 1.0, and 1.5 MHz operating frequencies.

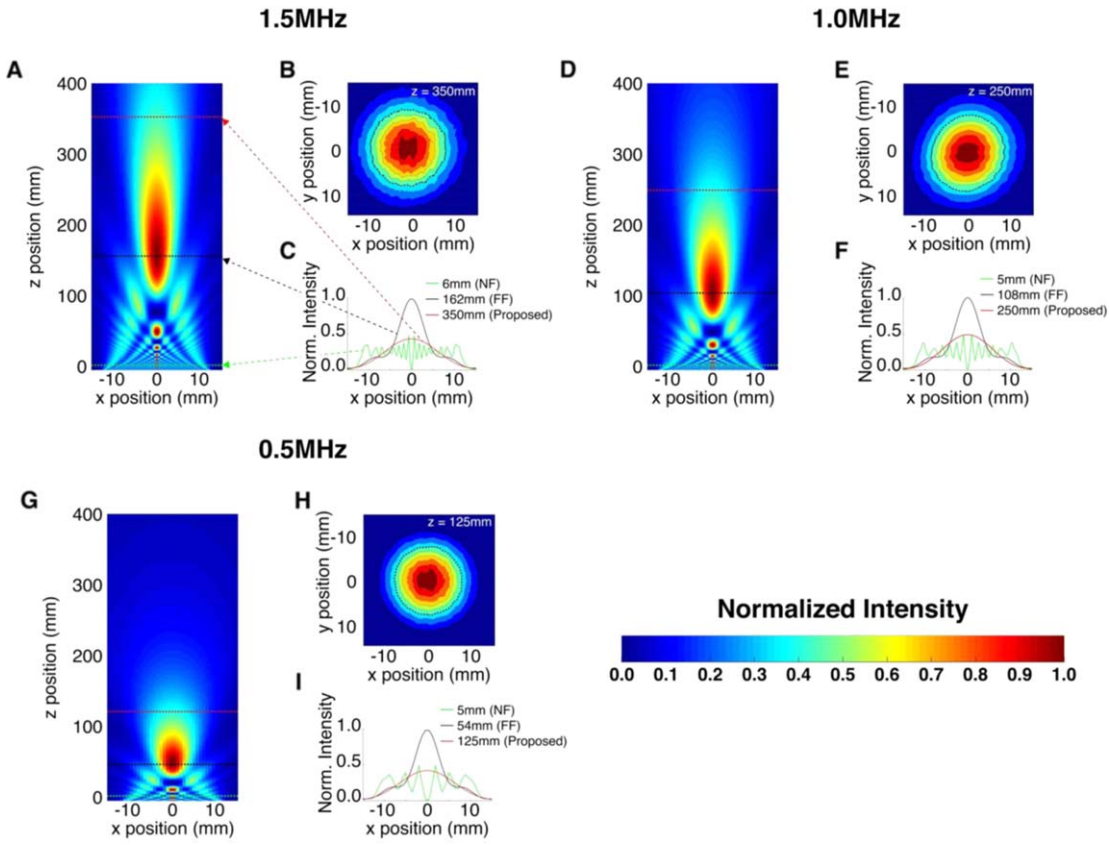

Figure 2. Simulated and measured acoustic fields from 25 mm diameter planar transducers at 1.5, 1.0, and 0.5 MHz frequency. Axial simulations (A), (D), (G) demonstrated a heterogeneous near-field and a more uniform far-field region for each frequency as well as an expected reduction in focal depth with reduced frequency. Transverse line traces of these simulations (C), (F), (I) further highlighted differences in intensity distribution with depth in the acoustic field. Arrows indicate the location at which each line trace was taken within the simulated acoustic field. Multiple peaks were observed in the near-field, a uniform but narrow distribution at the focus, and a uniform and broad distribution past the focus. The latter was chosen for the LIPUS configuration and cross-sectional intensity measurements (B), (E), (H) were taken at the proposed depth via hydrophone scanning. The region within the dotted line is $\geqslant$ 50% of the maximum intensity and represents the location where the cellular target was placed.

Predicted acoustic standoff distances of 125, 250, and 350 mm would yield 107.3%, 97.5%, and 82.9% coverage of the effective cell culture area within the FWHM for 0.5, 1.0, and 1.5 MHz operating frequencies, respectively (table 2 and figure 2). Hydrophone measurements of the acoustic field distributions from fabricated transducers at these standoff distances (figures 2(B), (E), (H)) yielded 133.23%, 104.7%, and 98.7% coverage, respectively over 1.91 cm^2 area, demonstrating the feasibility of delivering broad, FF acoustic energy covering greater than 80% of the effective cell culture area.

Evaluation of acoustic absorber

Sylgard 170, a biocompatible silicone [58], demonstrated the greatest attenuation coefficient (18.4 dB cm^{-1}) with minimal reflection from the surface at less than 5% (table 1). Absorber efficacy, as evaluated by pulse-echo measurements, demonstrated the elimination of reflections back toward the well-bottom, thereby minimizing the generation of standing waves within CCP wells. The reflection amplitude was reduced by 99.1% with the absorber in position (3.375Vpp versus 0.031Vpp).

US-beam uniformity at cell culture position

Surface plots of normalized intensity (figure 3) qualitatively demonstrate the heterogeneity of the beam profile in the NF compared to the more uniform profile in the FF. In addition, it is apparent that the introduction of a narrow-diameter 24-well CCP in the beam path increases the heterogeneity in both the NF and FF configurations. When replaced with a wide-diameter 6-well CCP, the intensity distribution is less uniform than with no plate, but more uniform than with the narrow-diameter 24-well CCP.

Quantitative measurements of uniformity for the FF configurations, as shown in figure 4, demonstrated an 80.3%–86.4% reduction in mean gradient magnitude and reduced standard deviation in gradient magnitude by 78.9%–93.7% when compared to corresponding NF configurations. The FF configuration including an alginate ring placed within a 6-well CCP (figure 3F) demonstrated a 60.1% reduction in mean gradient magnitude compared to the configuration with a 24-well CCP in at the same position (figure 3E) (0.10 ± 0.06 W cm^{-2} mm^{-1} versus 0.26 ± 0.16 W cm^{-2} mm^{-1}) and is similar to the no-plate

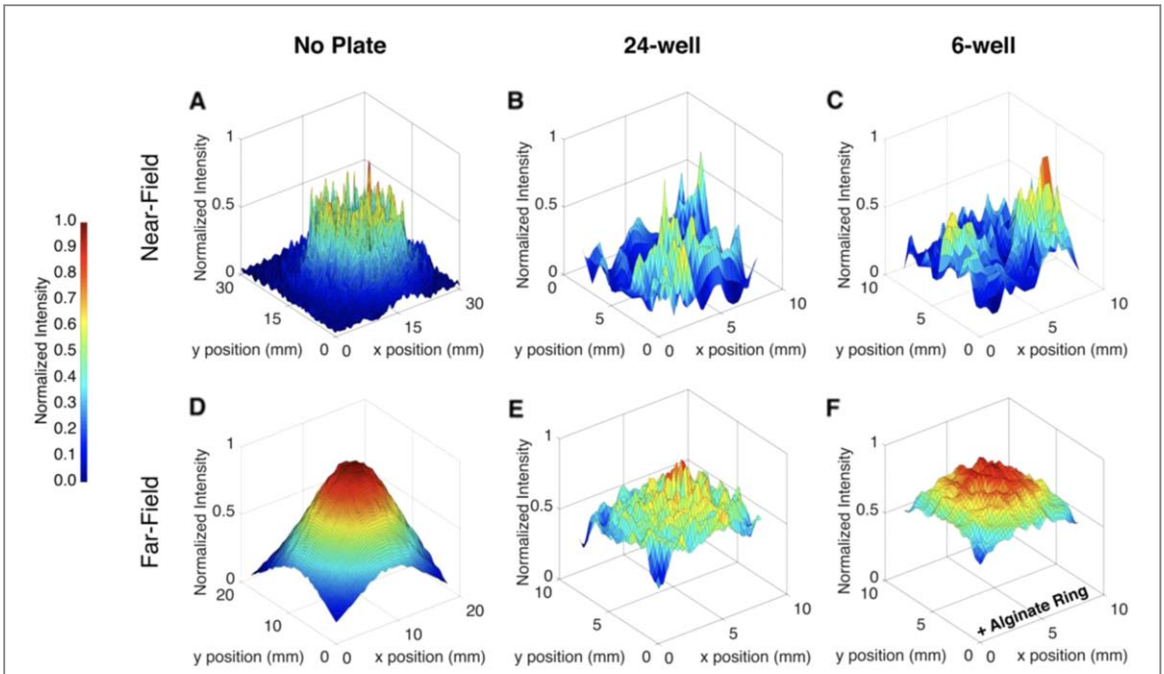

Figure 3. Surface plots depicting normalized intensity distributions measured via hydrophone scanning at the sample location (2 mm above the well bottom) in various commonly used *in-vitro* LIPUS configurations (A)–(E) and the custom configuration (F). Overall, the intensity distribution within the near-field (5 mm offset) (A)–(C) was extremely heterogeneous compared to the far-field (350 mm offset) (D)–(F). For both regions, there was more heterogeneity with a narrow-diameter 24-well plate compared to a wide-diameter 6-well plate. The custom configuration (F), which included an alginate ring inserted in a 6-well plate, had the most uniform intensity distribution compared to all other configurations that included a well-plate. Note that the plot for the far-field, 24-well plate setup has a single narrow peak in intensity gradient due to well-wall reflections, increasing the heterogeneity of its intensity field.

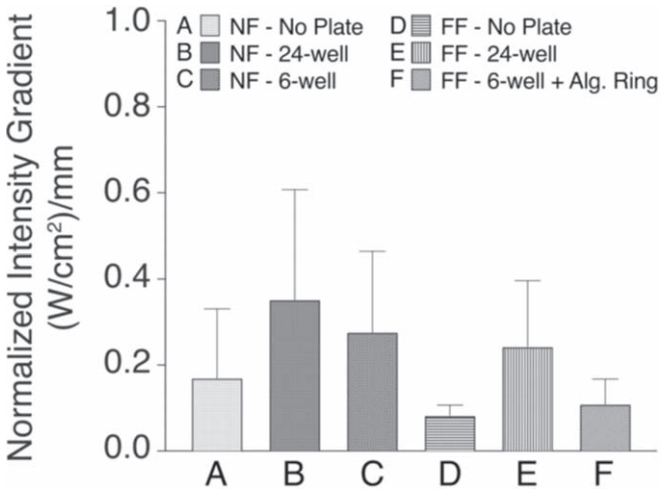

Figure 4. Acoustic field uniformity was quantified by measuring the intensity gradient and normalizing by the maximum value for each group. The intensity gradient of the custom *in-vitro* LIPUS configuration (F) was significantly less than all other configurations that included a well-plate (B), (C), (E). The normalized intensity gradient of each group was significantly different from all other groups ($p < 0.05$). Error bars represent standard deviation of the intensity gradient.

configuration (figure 3D) (0.08 ± 0.02 W cm^{-2} mm^{-1} versus 0.10 ± 0.06 W cm^{-2} mm^{-1}).

Temperature measurements

Temperature elevation measured within the well and absorber material during sonication at 1.5 MHz, demonstrated low temperature elevations within alginate beads of 0.81 ± 0.15°C, and 0.61 ± 0.31°C for the CCP-well bottom. Temperature rise was greatest within the acoustic absorber, with a temperature elevation of 2.32 °C $\pm$ 0.27 °C.

Extracellular matrix deposition

LIPUS-induced bioactivity was evaluated and compared to BMP-7 exposure (as a positive control) by hydroxyproline assay for quantification of total collagen content and by DMMB assay for quantification of sGAG content. Exposure to both treatments had a

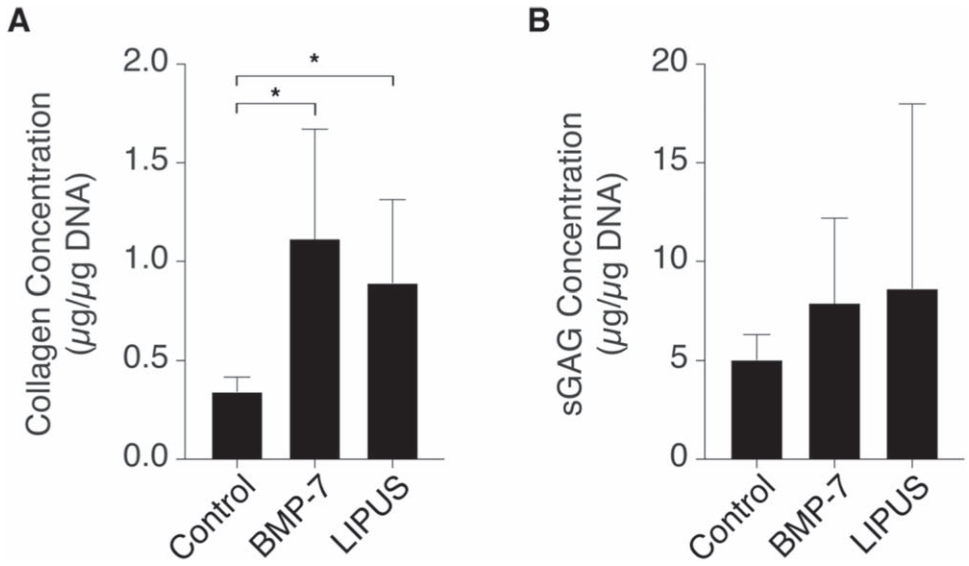

Figure 5. Quantification of extracellular matrix deposition. LIPUS and BMP-7 growth factor treatment upregulated collagen concentration by a similar magnitude and were both significantly greater than the nontreated control group ($^*p < 0.05$) (A). sGAG concentration was increased, but not significantly upregulated by LIPUS nor BMP-7 treatment (B). Both collagen and sGAG concentration were calculated as the sum of total collagen or sGAG content normalized by total DNA content in alginate beads. Error bars represent standard deviation of the collagen and sGAG concentration.

profound effect on collagen concentration compared to nontreated controls (figure 5A), with a 3.3-fold increase in the BMP-7 group ($1.12 \pm 0.55\ \mu g\ \mu g^{-1}$ DNA versus $0.34 \pm 0.07\ \mu g\ \mu g^{-1}$ DNA, $p = 0.03$), and a 2.6-fold increase in the LIPUS group ($0.89 \pm 0.42\ \mu g\ \mu g^{-1}$ DNA versus $0.34 \pm 0.07\ \mu g\ \mu g^{-1}$ DNA, $p = 0.03$). There was no significant difference in collagen concentration between the BMP-7 and LIPUS treatment groups, ($p = 0.47$). sGAG concentration was increased, but there was no significant difference between the BMP-7 and control groups ($7.91 \pm 4.23\ \mu g\ \mu g^{-1}$ DNA versus $5.03 \pm 1.26\ \mu g\ \mu g^{-1}$ DNA, $p = 0.77$) nor the LIPUS and control groups ($8.60 \pm 9.41\ \mu g\ \mu g^{-1}$ DNA versus $5.03 \pm 1.26\ \mu g\ \mu g^{-1}$ DNA, $p = 0.68$) (figure 5B).

Discussion

In this study, we investigated design parameters for an *in-vitro* LIPUS exposimetry system to deliver uniform FF acoustic energy to a distal target while mitigating several common acoustic artifacts. We identified the proper combination of transducer dimensions, and acoustic standoff distance for various low frequency (0.5–1.5 MHz) sources to deliver broad, uniform US energy to a target sample area within a CCP well. This configuration, combined with an optimized absorber and alginate ring design, enabled delivery of 50% prescribed I_{SATA} across the target region within the CCP well. Using the final design, we treated bovine IVD cells over the course of several days then measured collagen content and found that FF LIPUS exposure upregulates collagen production in IVD cells comparable to BMP-7 growth factor treatment.

Typically, *in-vitro* LIPUS systems include cells cultured in polystyrene CCPs placed directly above a planar transducer [28, 42]. When comparing intensity distributions at various axial distances, we observed extremely heterogeneous intensity fields directly above the transducer and a more uniform field at the transducer's natural focus (i.e. FF transition). However, the intensity distribution at this location manifests as a narrow peak with a FWHM intensity of < 8.5 mm for each transducer frequency considered. At further distances within the FF, the intensity field demonstrated broader peaks, with a 2-fold increase in FWHM intensity. These data suggested that uniform, broad exposure can be achieved at positions past the focus, within the diverging FF.

The presence of standing waves originating at the liquid-air interface of *in-vitro* US exposure systems can increase the pressure amplitude at the cell culture position by up to 2-fold, or decrease by up to 50%, which leads to uncertainty in the exposure conditions and could either significantly reduce cell viability or considerably reduce the expected therapeutic dose, resulting in a less predictable therapeutic effect [33, 59]. By addition of the custom absorber, the formation of standing waves within the CCP well would be negligible. Since the total energy delivered to the target can vary widely due to standing waves, eliminating them is essential for the success of future parametric studies.

Initial acoustic field simulations and hydrophone measurements gave insight into the acoustic intensity field devoid of obstruction; however, as previously mentioned, cells are typically cultured within the confinement of a CCP well. Therefore, a more relevant

analysis requires assessing the intensity field just beyond CCP-well bottom where the cells are located. By calculating the intensity gradient within this region, we have quantified the uniformity of the acoustic intensity field at the cell culture position within various common *in-vitro* configurations and demonstrated that adaptations to these configurations can greatly reduce beam heterogeneity in terms of intensity gradient magnitude. We found that the configuration with a 24-well CCP placed in the NF had the greatest intensity gradient, suggesting that cells treated using this configuration are particularly susceptible to heterogeneous mechanical stimulation and heating throughout the sample. Previous studies have suggested that differences in bioeffects may be explained by the local heterogeneity in the intensity distribution when exposing cells within the transducer's NF [34]. The FF configuration with an alginate ring inside a 6-well CCP had the lowest intensity gradient. This finding aligns with previous literature which hypothesized that the use of a well larger than the diameter of the transducer would reduce heterogeneity by minimizing reflections from well-walls [33]. The addition of an acoustically transparent alginate ring constrains the cells within a region outside the influence of the well-wall reflections believed to contribute the heterogeneity in narrow-welled configurations.

It is well accepted that exposure to US-energy has a therapeutic effect on several musculoskeletal tissues; however, the common presence of uncontrolled, US-induced heating of the CCP-plastic (by attenuation as well as heat transfer through direct contact with the transducer), and subsequently the sample, suggests that the mechanism of these effects may not be exclusively due to mechanical effects. Previous studies have shown that temperature elevation greater than 3 °C is enough to induce bioeffects on cell cultures and can be reached even when delivering low intensities (e.g. $I_{SATA} = 32\ mW\ cm^{-2}$) [30, 31, 60]. US-induced temperature elevation within the cell culture media as well as the well-walls and bottom of a CCP has been investigated for monolayer cultures [30, 61]; however, those observations may not be relevant for understanding heating effects on cells encapsulated in 3D-constructs such as sodium alginate beads. In the LIPUS system developed herein, which included a circulating water bath and acoustic absorber, we observed negligible average temperature elevations of < 1.0 °C within the alginate beads and CCP-well bottom, which is appreciably less than the temperature elevations previously reported in direct-contact systems [30] and demonstrates the ability to remove confounding temperature effects in LIPUS *in-vitro* studies.

For validation, bovine AF cells were exposed to LIPUS using the FF exposimetry system. Results demonstrated that collagen production was significantly greater than the control group when treated with BMP-7 (3.3-fold) or LIPUS (2.6-fold); however, there was no significant difference between LIPUS treatment and BMP-7 treatment. The findings demonstrate that uniform, FF LIPUS exposure, while eliminating significant temperature elevation and standing waves, can promote increased extracellular matrix production in bovine IVD cells *in-vitro* at a magnitude similar to that of growth factor treatment. This increase in collagen content with LIPUS treatment aligns with previous studies which have demonstrated a 1.3-fold increase in total collagen in human annulus fibrosus cells [22] and fibroblast cells treated with LIPUS in the NF [47]. Our preliminary gene expression data suggest that both LIPUS and BMP-7 treatment regulate collagen I and II expression in AF cells at similar magnitudes. These results align with previous work [22, 62] and suggest that LIPUS may stimulate the production of major fibrillar collagens of the IVD, which are important for maintaining its structural integrity. Although this study has not differentiated between ratios of collagen I and collagen II levels for LIPUS and BMP-7, this could be further investigated in future studies to optimize LIPUS exposure levels by immunohistostaining or western blot analysis.

Overall, the results indicate that uniform, FF acoustic energy fields can be delivered to 3D cellular constructs cultured in standard CCP-wells and enclosed by an alginate ring spacer at frequencies at and below 1.5 MHz with negligible heating. Additionally, we demonstrate that FF LIPUS exposure increases collagen content in IVD cells, suggesting that LIPUS may be a potential therapeutic for stimulating repair of tissues deep within the body such as the IVD. Further investigations are needed to elucidate the effect of varying LIPUS dose parameters on the cell response and to optimize the benefits of LIPUS treatment in an IVD-tissue repair context.

Acknowledgments

This material is based upon work supported by the National Science Foundation Graduate Research Fellowship Program under Grant No. 1650113. This work was also supported in part by NIH R21EB024347.

ORCID iDs

Devante A Horne https://orcid.org/0000-0002-4829-0508
Matthew S Adams https://orcid.org/0000-0001-8494-2684

References

[1] Escoffre J M and Bouakaz A (ed) 2016 *Therapeutic Ultrasound* (*Advances in Experimental Medicine and Biology* 880) (Switzerland: Springer International Publishing) (https://doi.org/10.1007/978-3-319-22536-4)
[2] Hersh D S *et al* 2016 Emerging applications of therapeutic ultrasound in neuro-oncology: moving beyond tumor ablation *Neurosurgery* **79** 643–54
[3] Jiang X *et al* 2019 A review of low-intensity pulsed ultrasound for therapeutic applications *IEEE Transactions on Biomedical Engineering* **66** 2704–18

[4] Chen C *et al* 2019 Effect of low-intensity pulsed ultrasound after autologous adipose-derived stromal cell transplantation for bone-tendon healing in a rabbit model *Am J Sports Med* **47** 942–53

[5] Sheybani N D and Price R J 2019 Perspectives on recent progress in focused ultrasound immunotherapy *Theranostics* **9** 7749–58

[6] Baker K G, Robertson V J and Duck F A 2001 A review of therapeutic ultrasound: biophysical effects *Physical Therapy* **81** 1351–58

[7] Khanna A *et al* 2008 The effects of LIPUS on soft-tissue healing: a review of literature *British Medical Bulletin* **89** 169–82

[8] Martinez de Albornoz P *et al* 2011 The evidence of low-intensity pulsed ultrasound for *in vitro*, animal and human fracture healing *British Medical Bulletin* **100** 39–57

[9] Xin Z *et al* 2016 Clinical applications of low-intensity pulsed ultrasound and its potential role in urology *Transl Androl Urol* **5** 255–66

[10] Kristiansen T K *et al* 1997 Accelerated healing of distal radial fractures with the use of specific, low-intensity ultrasound—A multicenter, prospective, randomized, double-blind, placebo-controlled study *J Bone Joint Surg Am* **79A** 961–73

[11] Yang R-S *et al* 2005 Regulation by ultrasound treatment on the integrin expression and differentiation of osteoblasts *Bone* **36** 276–83

[12] Bhandari M *et al* 2009 Low-intensity pulsed ultrasound: fracture healing *Indian Journal of Orthopaedics* **43** 132

[13] Naruse K *et al* 2010 Prolonged endochondral bone healing in senescence is shortened by low-intensity pulsed ultrasound in a manner dependent on COX-2 *Ultrasound in Medicine & Biology* **36** 1098–108

[14] Pounder N M and Harrison A J 2008 Low intensity pulsed ultrasound for fracture healing: a review of the clinical evidence and the associated biological mechanism of action *Ultrasonics* **48** 330–8

[15] Cook S D *et al* 2001 Improved cartilage repair after treatment with low-intensity pulsed ultrasound *Clinical Orthopaedics and Related Research®* **391** S231–243

[16] Yeung C K, Guo X and Ng Y F 2006 Pulsed ultrasound treatment accelerates the repair of Achilles tendon rupture in rats *J Orthop Res* **24** 193–201

[17] Lu H *et al* 2008 Low-intensity pulsed ultrasound accelerated bone-tendon junction healing through regulation of vascular endothelial growth factor expression and cartilage formation *Ultrasound in Medicine & Biology* **34** 1248–60

[18] Lu H *et al* 2017 Low-intensity pulsed ultrasound accelerates bone-tendon junction healing: a partial patellectomy model in rabbits *Am J Sports Med* **34** 1287–96

[19] Qin L *et al* 2006 Low-intensity pulsed ultrasound accelerates osteogenesis at bone-tendon healing junction *Ultrasound in Medicine & Biology* **32** 1905–11

[20] Demir H *et al* 2004 Comparison of the effects of laser, ultrasound, and combined laser + ultrasound treatments in experimental tendon healing *Lasers Surg Med* **35** 84–9

[21] Fu S C *et al* 2008 Low-intensity pulsed ultrasound on tendon healing: a study of the effect of treatment duration and treatment initiation *Am J Sports Med* **36** 1742–9

[22] Chen M H *et al* 2015 Low-intensity pulsed ultrasound stimulates matrix metabolism of human annulus fibrosus cells mediated by transforming growth factor β1 and extracellular signal-regulated kinase pathway *Connective Tissue Research* **56** 219–27

[23] Zhou X-Y *et al* 2017 Low-intensity pulsed ultrasound-induced spinal fusion is coupled with enhanced calcitonin gene-related peptide expression in rat model *Ultrasound in Medicine & Biology* **43** 1486–93

[24] Atherton P, Lausecker F, Harrison A and Ballestrem C 2017 Low-intensity pulsed ultrasound promotes cell motility through vinculin-controlled Rac1 GTPase activity *Journal of Cell Science* **130** 2277–91

[25] Xu X *et al* 2016 LIPUS promotes spinal fusion coupling proliferation of type H microvessels in bone *Sci. Rep.* **6** 1–10

[26] Montalti C S *et al* 2013 Effects of low-intensity pulsed ultrasound on injured skeletal muscle *Braz. J. Phys. Ther.* **17** 343–50

[27] Hui C F F *et al* 2011 Low-intensity pulsed ultrasound enhances posterior spinal fusion implanted with mesenchymal stem cells-calcium phosphate composite without bone grafting *SPINE* **36** 1010–6

[28] Miyamoto K *et al* 2005 Exposure to pulsed low intensity ultrasound stimulates extracellular matrix metabolism of bovine intervertebral disc cells cultured in alginate beads *SPINE* **30** 2398–405

[29] Zhou S *et al* 2004 Molecular mechanisms of low intensity pulsed ultrasound in human skin fibroblasts *J. Biol. Chem.* **279** 54463–9

[30] Leskinen J J and Hynynen K 2012 Study of factors affecting the magnitude and nature of ultrasound exposure with *in vitro* set-ups *Ultrasound in Medicine & Biology* **38** 777–94

[31] Leskinen J J, Olkku A and Mahonen A 2014 Nonuniform temperature rise in *in vitro* osteoblast ultrasound exposures with associated bioeffect *IEEE Transactions on Ultrasonics, Ferroelectrics, and Frequency Control* **61** 920–7

[32] Marvel S *et al* 2010 The development and validation of a lipus system with preliminary observations of ultrasonic effects on human adult stem cells *IEEE Transactions on Ultrasonics, Ferroelectrics, and Frequency Control* **57** 1977–84

[33] Hensel K, Mienkina M P and Schmitz G 2011 Analysis of ultrasound fields in cell culture wells for *in vitro* ultrasound therapy experiments *Ultrasound in Medicine & Biology* **37** 2105–15

[34] Fung C-H *et al* 2014 Osteocytes exposed to far field of therapeutic ultrasound promotes osteogenic cellular activities in pre-osteoblasts through soluble factors *Ultrasonics* **54** 1358–65

[35] Puts R, Ruschke K and Ambrosi T H 2016 A Focused Low-Intensity Pulsed Ultrasound (FLIPUS) system for cell stimulation: physical and biological proof of principle *IEEE Transactions on Ultrasonics, Ferroelectrics, and Frequency Control* **63** 91–100

[36] Leskinen J J *et al* 2008 Genome-wide microarray analysis of MG-63 osteoblastic cells exposed to ultrasound *Biorheology* **45** 345–54

[37] Kinoshita M and Hynynen K 2007 Key factors that affect sonoporation efficiency in *in vitro* settings: the importance of standing wave in sonoporation *Biochemical and Biophysical Research Communications* **359** 860–5

[38] Ocheltree K B and Frizzell L A 1989 Sound field calculation for rectangular sources *IEEE Transactions on Ultrasonics, Ferroelectrics, and Frequency Control* **36** 242–8

[39] Adams M S *et al* 2017 Integration of deployable fluid lenses and reflectors with endoluminal therapeutic ultrasound applicators: Preliminary investigations of enhanced penetration depth and focal gain *Med. Phys.* **44** 5339–56

[40] Ophir J, McWhirt R E, Maklad N F and Jaeger P M 1985 A narrowband pulse-echo technique for *in vivo* ultrasonic attenuation estimation *IEEE Trans. Biomed. Eng.* **32** 205–12

[41] Parvizi J *et al* 1999 Low-intensity ultrasound stimulates proteoglycan synthesis in rat chondrocytes by increasing aggrecan gene expression *J. Orthop. Res.* **17** 488–94

[42] Iwashina T *et al* 2006 Low-intensity pulsed ultrasound stimulates cell proliferation and proteoglycan production in rabbit intervertebral disc cells cultured in alginate *Biomaterials* **27** 354–61

[43] Schumann D *et al* 2006 Treatment of human mesenchymal stem cells with pulsed low intensity ultrasound enhances the chondrogenic phenotype *in vitro Biorheology* **43** 431–43

[44] Tang X *et al* 2019 Pulsed electromagnetic fields reduce interleukin-6 expression in intervertebral disc cells via nuclear factor-$\kappa\beta$ and mitogen-activated protein kinase p38 pathways *SPINE* **44** E1290–7

[45] Subramanian A, Budhiraja G and Sahu N 2017 Chondrocyte primary cilium is mechanosensitive and responds to low-intensity-ultrasound by altering its length and orientation *The International Journal of Biochemistry & Cell Biology* **91** 60–64

[46] Lee H-P *et al* 2017 Mechanical confinement regulates cartilage matrix formation by chondrocytes *Nat. Mater.* **16** 1243–51
[47] Bohari S P, Grover L M and Hukins D W 2012 Pulsed-low intensity ultrasound enhances extracellular matrix production by fibroblasts encapsulated in alginate *Journal of Tissue Engineering* **3** 1–7
[48] Ouyang A *et al* 2016 Effects of cell type and configuration on anabolic and catabolic activity in 3D co-culture of mesenchymal stem cells and nucleus pulposus cells *J. Orthop. Res.* **35** 61–73
[49] Miller S L *et al* 2016 Pulsed electromagnetic field (PEMF) treatment reduces expression of genes associated with disc degeneration in human intervertebral disc cells *The Spine Journal* **16** 770–6
[50] Wang Z, Hutton W C and Yoon S T 2013 ISSLS Prize winner: effect of link protein peptide on human intervertebral disc cells *SPINE* **38** 1501–507
[51] Masuda K *et al* 2003 Recombinant osteogenic protein-1 upregulates extracellular matrix metabolism by rabbit annulus fibrosus and nucleus pulposus cells cultured in alginate beads *J. Orthop. Res.* **21** 922–30
[52] Zhang X J, Hu Z M, Hao J and Shen J L 2016 Low intensity pulsed ultrasound promotes the extracellular matrix synthesis of degenerative human nucleus pulposus cells through FAK/PI3K/Akt pathway *SPINE* **41** E248–54
[53] Kobayashi Y, Sakai D, Iwashina T and Iwabuchi S 2009 Low-intensity pulsed ultrasound stimulates cell proliferation, proteoglycan synthesis and expression of growth factor-related genes in human nucleus pulposus cell line *European Cells and Materials* **17** 15–22
[54] Thonar E, An H and Masuda K 2002 Compartmentalization of the matrix formed by nucleus pulposus and annulus fibrosus cells in alginate gel *Biochem Soc Trans* **30** 874–878
[55] Bron J L *et al* 2008 Repair, regenerative and supportive therapies of the annulus fibrosus: achievements and challenges *Eur. Spine J.* **18** 301–313
[56] Augst A D, Kong H J and Mooney D J 2006 Alginate hydrogels as biomaterials *Macromol Biosci* **6** 623–633
[57] Enobakhare B O, Bader D L and Lee D A 1996 Quantification of sulfated glycosaminoglycans in chondrocyte/alginate cultures, by use of 1,9-dimethylmethylene blue *Anal Biochem* **243** 189–191
[58] la Cour M F *et al* 2014 Investigation of PDMS as coating on CMUTs for imaging *2014 IEEE Int. Ultrasonics Symp. (Chicago, IL, USA)* 2584–2587
[59] Karshafian R *et al* 2009 Sonoporation by ultrasound-activated microbubble contrast agents: effect of acoustic exposure parameters on cell membrane permeability and cell viability *Ultrasound in Medicine & Biology* **35** 847–860
[60] Han S I *et al* 2002 Mild heat shock induces cyclin D1 synthesis through multiple Ras signal pathways *FEBS Letters* **515** 141–145
[61] Sena K *et al* 2005 Early gene response to low-intensity pulsed ultrasound in rat osteoblastic cells *Ultrasound in Medicine & Biology* **31** 703–708
[62] Kim J-S *et al* 2010 Insulin-like growth factor 1 synergizes with bone morphogenetic protein 7-mediated anabolism in bovine intervertebral disc cells *Arthritis & Rheumatism* **62** 3706–3715